

Article

Ice-Templating for the Elaboration of Oxygen Permeation Asymmetric Tubular Membrane with Radial Oriented Porosity

Cyril Gaudillere, Julio Garcia-Fayos , Jorge Plaza and José M. Serra * 

Instituto de Tecnología Química (Universitat Politècnica de València – Consejo Superior de Investigaciones Científicas), Av. Naranjos s/n, E-46022 Valencia, Spain; cgaudi@itq.upv.es (C.G.); jugarfa@itq.upv.es (J.G.-F.); jorplabe@itq.upv.es (J.P.)

* Correspondence: jmserra@itq.upv.es; Fax: +34-963-877-809

Received: 6 February 2019; Accepted: 28 March 2019; Published: 2 April 2019



Abstract: An original asymmetric tubular membrane for oxygen production applications was manufactured in a two-step process. A 3 mol% Y_2O_3 stabilized ZrO_2 (3YSZ) porous tubular support was manufactured by the freeze-casting technique, offering a hierarchical and radial-oriented porosity of about 15 μm in width, separated by fully densified walls of about 2 μm thick, suggesting low pressure drop and boosted gas transport. The external surface of the support was successively dip-coated to get a $Ce_{0.8}Gd_{0.2}O_{2-\delta} - 5mol\%Co$ (CGO-Co) interlayer of 80 μm in thickness and an outer dense layer of $La_{0.6}Sr_{0.4}Co_{0.2}Fe_{0.8}O_{3-\delta}$ (LSCF) with a thickness of 30 μm . The whole tubular membrane presents both uniform geometric characteristics and microstructure all along its length. Chemical reactivity between each layer was studied by coupling X-Ray Diffraction (XRD) analysis and Energy Dispersive X-Ray spectroscopy (EDX) mapping at each step of the manufacturing process. Cation interdiffusion between different phases was discarded, confirming the compatibility of this tri-layer asymmetric ceramic membrane for oxygen production purposes. For the first time, a freeze-cast tubular membrane has been evaluated for oxygen permeation, exhibiting a value of $0.31 mL \cdot min^{-1} \cdot cm^{-2}$ at 1000 °C under air and argon as feed and sweep gases, respectively. Finally, under the same conditions and increasing the oxygen partial pressure to get pure oxygen as feed, the oxygen permeation reached $1.07 mL \cdot min^{-1} \cdot cm^{-2}$.

Keywords: ice templating; freeze-casting; tubular asymmetric membrane; oxygen permeation; perovskite material

1. Introduction

Sustainable production of pure oxygen is one of the most relevant challenges for environmental and industrial purposes. Widely used by the steel industry, power generation and chemical industry, about 100 million tons of pure oxygen are produced annually by cryogenic distillation and Pressure Swing Adsorption (PSA). Both processes have been widely studied and improved, but the large size of the industrial complex needed for cryogenic distillation and the low purity of the oxygen produced by PSA are a drawback for the implementation of small scale applications [1]. Ceramic asymmetric MIEC (Mixed Ionic and Electronic Conductors) membranes operating at high temperature offer higher energy efficiency and lower production costs than state-of-the-art technologies, establishing them as a suitable alternative for industrial oxygen production. Several research groups are devoted to the improvement of this technology for an up-scaling to industry, where the most effective configuration to date is composed by a porous ceramic support covered by a thin dense layer of a MIEC material. This dense layer acts as a sieve that will segregate the oxygen from the rest of constituents in air.

These membranes can be enhanced by improving the ambivalent conductivity of the MIEC material, by modifying the manufacture process to optimize the porous support architecture or by reducing the dense layer thickness using coating techniques such as RF sputtering or Chemical Vapor Deposition. Some studies considering the integration of MIEC membranes for O₂ production within industrial processes established oxygen flux targets of at least 10 mL·min⁻¹·cm⁻² for achieving a techno-economic feasibility on the considered applications [2,3].

Regarding their composition, ABO_{3-δ} perovskite-related materials are widely implemented in oxygen separation membranes due to their intrinsic properties. Attention has been focused particularly on La_{0.6}Sr_{0.4}Co_{0.2}Fe_{0.8}O_{3-δ} (LSCF) as a result of its high mixed conductivity and promising stability under CO₂-containing atmospheres [4,5].

Prior to this work, a new LSCF planar porous support architecture based on the *freeze-casting* process [6] has been developed. This technique consists in freezing a ceramic liquid suspension rapidly to form crystals of the solvent, displacing ceramic particles as they grow, resulting in the formation of channels with a specific geometry. Then, the solvent crystals are sublimated under both low temperature and pressure, to finally sinter the sample to end the process. The obtained structure is highly porous with oriented channels corresponding to the replica of the solvent crystals along the propagation direction of the solid–liquid interface [7]. It has been shown that the obtained freeze-cast porous support presents a total porosity of about 58% and the resulting membrane after screen-printing of a thick dense top-layer on the top of it exhibits unprecedented oxygen permeation values due to the optimization of gas transport through the hierarchical porosity of the support [6,8].

Regarding the design of asymmetric membrane, two configurations are considered in literature. On the one hand, disk-shaped or planar configurations are the most studied in literature, presenting advantages related to manufacturing simplicity rapid evaluation of permeation values. For this design, the porous support is generally developed by uniaxial pressing and subsequent sintering of the powder, while the dense top layer is deposited using conventional coating techniques such as screen-printing or tape casting [5,9,10]. Nevertheless, from an industrial point of view such configuration presents limited membrane area for oxygen permeation and edge leakage issues [11]. The required membrane surface to reach the targeted oxygen permeation fluxes could be obtained by stacking multiple planar membranes, which would bring new challenges related to sealing between membranes or pressure resistance of the ensemble.

On the other hand, tubular configuration membranes are an improvement on the planar design due to its improved strength and surface area, yet they are far more challenging to shape. In addition, tubular membranes are usually manufactured by extrusion or isostatic pressing [12–15], which are heavier to implement than conventional shaping techniques (uniaxial pressing, tape casting). Nevertheless, a higher surface area/volume ratio, an easier scale-up than disk-shaped membrane and simpler sealing in the cold zone of the setup leads to an increasing interest on developing tubular membranes. This configuration would allow to fulfil the targeted oxygen permeation values in a reduced space and therefore become worthy to be set up for small scale applications. Up to now, few studies of tubular asymmetric MIEC membranes are reported mainly due to the difficulty in manufacture, but generally oxygen permeation values obtained are much higher than planar configuration tests [14–17]. The first attempts for implementing ice-templating to elaborate tubular asymmetric membranes were conducted by Moon et al. [18,19] and most recently by Liu et al. [20] and Seuba et al. [21]. Despite the impressive results obtained from these studies and the demonstration of ice-templating as a useful technique for the production of ceramic tubes with hierarchically oriented porosity, there are no studies in literature where freeze-cast tubes are applied for oxygen production in asymmetric membranes.

In accordance with all these observations, this work focuses on the implementation of freeze-casting to manufacture tubular membranes and on its relevance as an oxygen production alternative. The material chosen for the freeze-cast porous support is the 3 mol% yttria stabilized zirconia (3YSZ), combined with the highly conductive LSCF presented above as the MIEC layer. Due to the chemical incompatibility of these two materials at high temperature, a protective interlayer of the Ce_{0.8}Gd_{0.2}O_{2-δ}

(CGO) fluorite material is applied to minimize phase interactions [22]. Indeed, several studies detail the chemical reaction of the LSCF perovskite with the yttria-stabilized zirconia (YSZ) fluorite material where the formation of insulating pyrochlore phases like $\text{La}_2\text{Zr}_2\text{O}_7$ occur, impairing the membrane conductivity and stability [23]. CGO is often used as a protective interlayer between LSCF and YSZ materials, even though literature reveals that there is also a weak interaction between YSZ and CGO phases. It has been reported that Zr cations can diffuse into the CGO fluorite structure to modify its cubic-like fluorite structure. Nevertheless, only a slight decrease in the electrical conductivity is associated to this diffusion and no insulating phase was reported [24]. Moreover, the addition of a CGO interlayer turns out to benefit both the shaping and the mechanical integrity of the membrane during its production. In addition, this material presents a thermal expansion coefficient (TEC) of $12.5 \times 10^{-6} \text{ K}^{-1}$ [25], ranging between $11.78 \times 10^{-6} \text{ K}^{-1}$ of 3YSZ [26] and $18.4 \cdot 10^{-6} \text{ K}^{-1}$ of LSCF [27], thus serving as a buffer during the thermal cycling in operating conditions.

2. Materials and Methods

Asymmetric tubular membrane fabrication: The $\text{La}_{0.6}\text{Sr}_{0.4}\text{Co}_{0.2}\text{Fe}_{0.8}\text{O}_{3-\delta}$ (LSCF) and the $\text{Ce}_{0.8}\text{Gd}_{0.2}\text{O}_{2-\delta}$ (CGO) powders were provided by Oerlikon-Metco and Treibacher, respectively. Before use, all powders were ball-milled in acetone for 48 h to ensure homogeneity of the particle size. Then, the CGO powder was impregnated with cobalt nitrate hexahydrate (Sigma-Aldrich, St. Louis, MO, USA) to get a final 5 mol% of metallic cobalt, which will act as a sintering aid [28–30]. A calcination step at 400 °C for 3 h was then realized to remove precursors. The 3YSZ porous tubular support was produced by ice-templating using the formula that follows: Ceramic powder (40–50 wt %), water (30–40 wt %) as solvent, a polyacrylate-based dispersing agent (1–4 wt %) and polyethylene glycol 4000 (1–4 wt %) (Sigma-Aldrich). A defined volume of the previously homogenized slurry was poured into a 20 mm in diameter and 200 mm long metallic cylindrical mold supported by a Teflon disc while an ice stick was placed in the middle of the mold (Figure 1). The ice stick will serve as a template of the inner diameter after ice removal by freeze-drying. The length of the sample depends exclusively on the amount of slurry poured into the mold. The mold was placed into a liquid nitrogen bath and the freezing of the slurry took place. After the cast was completely frozen, the sample was removed from the mold and sublimated by freeze drying at -53 °C and reduced pressure for 24 h using a Scanvac commercial freeze dryer. The sample was then pre-sintered at 1150 °C/6 h in air to end up with a porous support that could be easily handled to then dip coat the MIEC layers. Dip coating inks were prepared by mixing a 1:1 weight ratio of the ceramic powders (CGO-Co or LSCF) and an ethylcellulose (6% wt.) solution in terpineol, respectively, in a three roll mill. Then, the CGO-Co layer is dip-coated over the outer surface of the porous 3YSZ sample and dried at 220 °C/1 h. The LSCF layer was then dip-coated over the CGO-Co hardened layer and dried at 220 °C/1 h. The final sintering step is performed at 1400 °C/6 h in air, densifying the LSCF top-layer, turning it into a complete gas-tight membrane.

Microscopy study: The microscopic study of the asymmetric membrane was completed using a Jeol JSM 6300 Scanning Microscope Jeol with an acceleration voltage of 20 kV.

XRD analysis: Powder reactivity between 3YSZ and LSCF powders has been studied by intimately mixing both powders and annealing at 1400 °C/6 h, simulating the final sintering step of the tubular membrane process. The powder ratio was 50:50 wt %.

Permeation test details: Permeation tests were performed in a lab-scale quartz reactor under a dead-end tubular membrane configuration, i.e., one end of the tubular membrane was sealed to an alumina tube for feed gas supplying, while the other end was covered and sealed to an YSZ dense disk. Vitreous sealant with the reference G018-218 from the company Schott AG were used in both seals. Synthetic air (21% v/v O_2) was fed on the internal porous support side of the tube through the alumina tube while the sweep gas was circulating through the outer surface, in contact with the LSCF (permeate side). Both gas streams were preheated to ensure the right temperature as it reached the membrane surface, fed at atmospheric pressure and individually mass flow controlled. The temperature was measured using a thermocouple directly in contact with the membrane's surface.

A proportional-integral-derivative (PID) controller was used to maintain temperature variations within 2 °C of the set point. Gas tightness of the tested LSCF sample was checked prior to the assembly in the reactor by means of a He-leak test. The permeate was analyzed at steady state by online gas chromatography using a micro-GC Varian CP-4900 (Varian BV, Middelburg, The Netherlands) equipped with Molsieve5A, Pora-Plot-Q glass capillary, and CP-sil modules. Membrane gas leak-free conditions were ensured by continuously monitoring the N₂ trace concentration in the permeate gas stream. During the conduction of the tests, the ratio between the O₂ leak flow and the O₂ flux was lower than 10%. The O₂ ascribed to leaks was subtracted from the O₂ concentration determined by the GC in the permeate, thus reflecting the actual membrane permeation. The data reported here were achieved at steady state after 1 h in the reaction stream. Each GC analysis was repeated three times to minimize the analysis error. The experimental error was below 0.5%

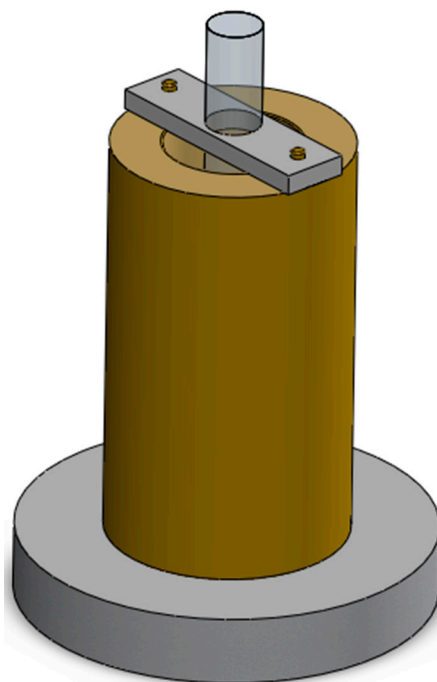


Figure 1. Sketch of the assembly used for the elaboration of freeze-cast porous tubular supports: A cylindrical metallic mold is supported over a Teflon disc while a Teflon strip placed on the upper part of the metallic mold centers the ice stick during the freezing process.

3. Results and Discussion

Preliminary Work

As mentioned in the introduction, the production of these membranes composed by different materials can induce cation interdiffusion at high temperature and thus the formation of insulating pyrochlore phase(s), leading to a decrease in conductivity and mechanical integrity of the piece. The presence of three different materials and two interfaces where reactivity can occur requires analyzing if an interlayer between the 3YSZ freeze-cast support and the LSCF outer layer is needed. For that, a mixture of both powders with a 50:50 wt % ratio has been prepared by intimate grinding and at 1400 °C/6 h, simulating the final densification thermal treatment of the membrane. The mixture was studied by means of XRD and compared with the 3YSZ and LSCF starting powders. Figure 2 details the XRD patterns of both starting powders and the LSCF/3YSZ mixture. Both original powders were well crystallized and had no secondary phases while a phase transformation was observed in the mixture of both powders, forming a pyrochlore phase at high temperature indexed as Sr₂Fe₂O₅ (identified by * on the pattern). The LSCF perovskite structure completely disappeared, whereas only the stronger peaks

associated to the 3YSZ structure could be indexed. This observation confirms previous work [23] and the necessity to apply an interlayer between 3YSZ and LSCF.

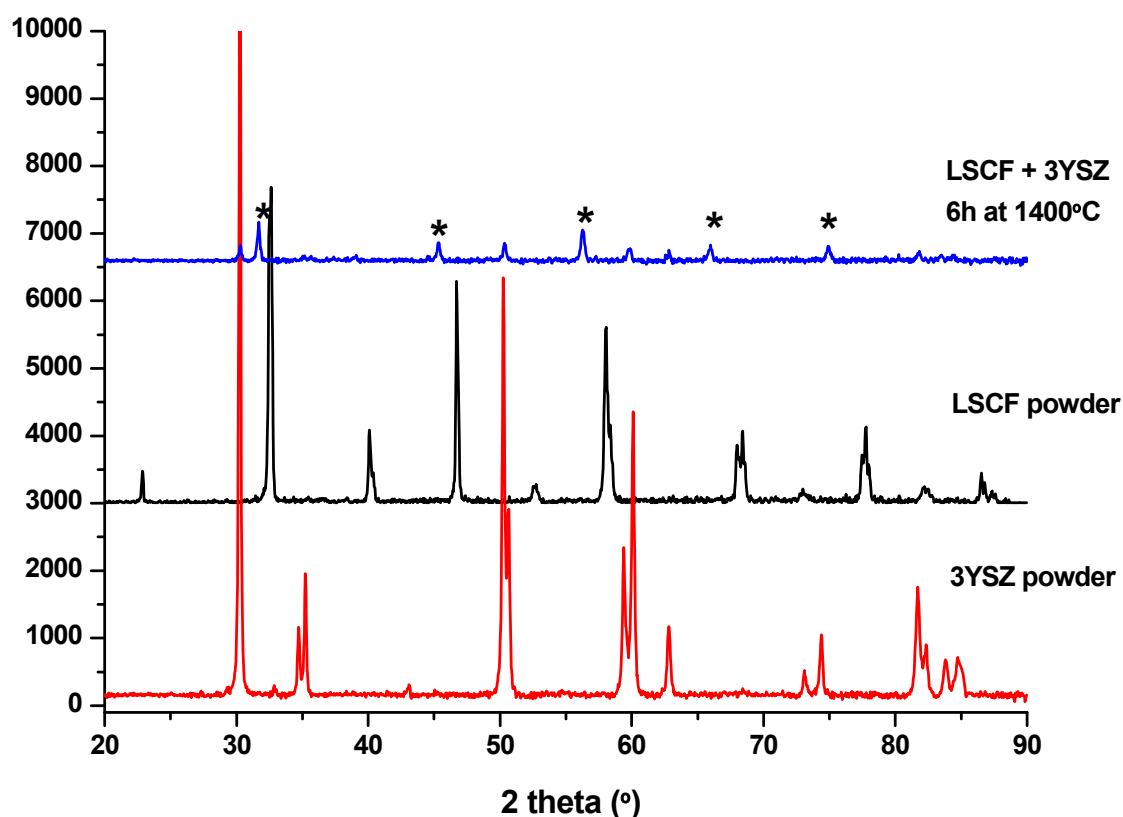


Figure 2. XRD patterns of the 3YSZ and $\text{La}_{0.6}\text{Sr}_{0.4}\text{Co}_{0.2}\text{Fe}_{0.8}\text{O}_{3-\delta}$ (LSCF) starting powders and of the mixture of both powders annealed at 1400 °C/6 h. Additional phase after reactivity test is marked by *.

Figure 3 displays photos of the asymmetric ceramic membrane at different stages of the process. Figure 3a shows a profile of the porous tubular support after pre-sintering at 1150 °C/6 h. The sample is 6 cm long and easy to handle. The same tubular porous support after both CGO-Co and LSCF dip-coating and drying is shown in Figure 3b, exhibiting a homogeneous outer layer all along the surface. Finally, the Figure 3c represents the final asymmetric membrane after sintering at 1400 °C/6 h. The LSCF top-layer presents a distinctive shiny appearance associated to densification of the surface. The final outer diameter of the sample is 15.6 mm all along the length of the tube while the inner diameter is 7.5 mm.

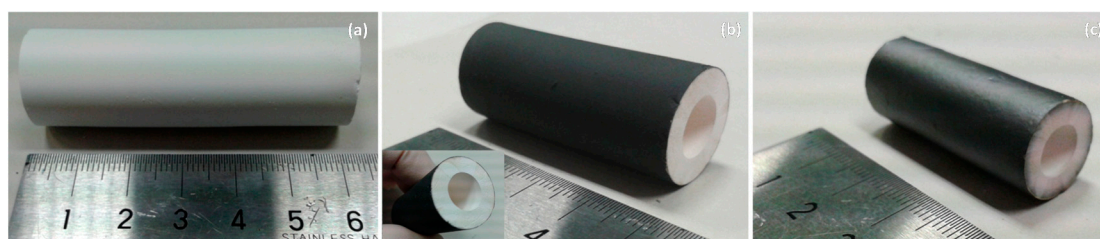


Figure 3. Pictures of the porous 3YSZ tubular freeze-cast support after pre-sintering 6 h at 1150 °C (a), after dip-coating of both the $\text{Ce}_{0.8}\text{Gd}_{0.2}\text{O}_{2-\delta}$ -5mol%Co (CGO-Co) interlayer and of the LSCF outer layer and drying at 220 °C (b), and after final sintering 6 h at 1400 °C (c).

4. Asymmetric Tubular Membrane Characterization

A full microscopic characterization to the 3YSZ tubular support has been carried out to fully understand its specific porosity. Figure 4 details the microstructure of the support by ice-templating. A global view is given in Figure 4a, where it is shown that the sample has a sheet-like microstructure stacked in parallel to the freezing direction all along the sample radius. A magnification of this phenomenon is given in Figure 4b,c. The ceramic walls have a thickness ranging from 1.5 to 2.5 μm , while the porosity between the two walls ranges from 12 to 15 μm . The total porosity of the freeze-cast YSZ support is in the range of 55–58%, as calculated by computational analysis of SEM cross-section images and by fluid saturation (Archimedes' Principle). Finally, the surface of a sintered 3YSZ wall is presented in Figure 4d, revealing good sintering and homogeneity with an average grain size of about 150 nm. Fully densified thin walls combined with large aligned porosity suggest low pressure drop and boosted gas transport for the porous support.

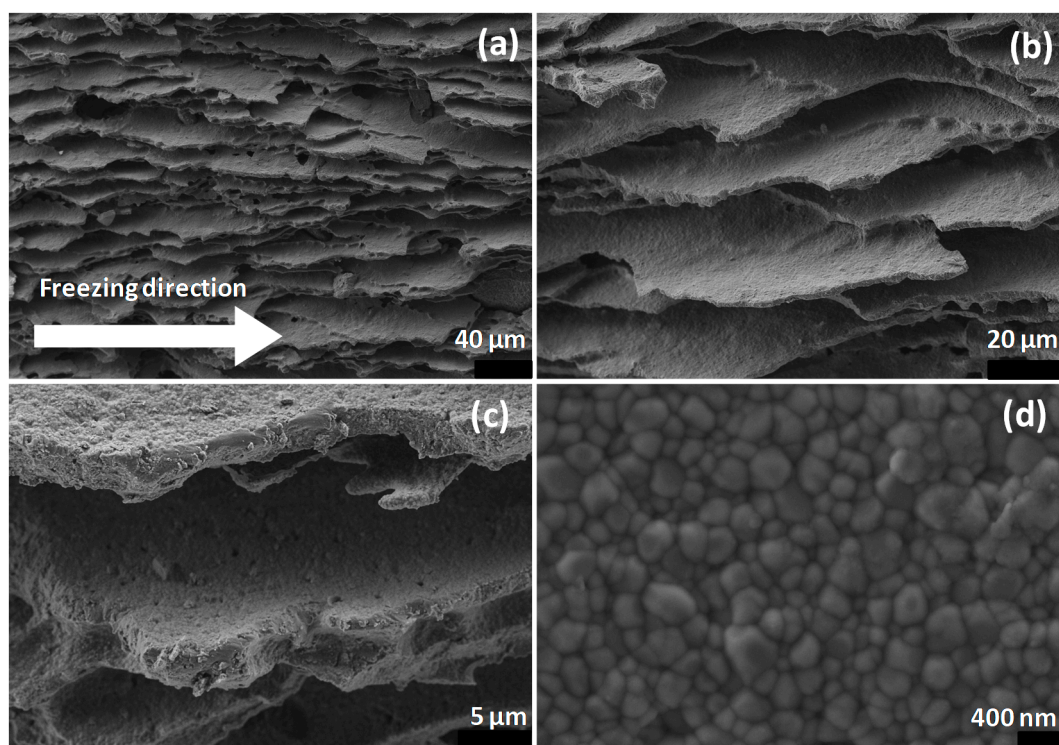


Figure 4. Cross-section SEM micrographs of the 3YSZ porous freeze-cast support with radial oriented porosity after sintering 6 h at 1400 °C (a), focus of the porous aligned architecture (b,c) and surface of the porosity wall (d).

A microscopic study of the whole asymmetric ceramic membrane is presented in Figure 5. The cross-section image of the sample in Figure 5a shows the curvatures of the inner and outer diameter, where two distinct layers are observable. The thickest one is the porous freeze-cast support, while the thin one is the dense LSCF layer. Cross-section close-ups of the outer part of the tube in Figure 5b,c clearly disclose three different layers. The first one shows the sheet-like porous 3YSZ, the second one shows the CGO-Co dip-coated interlayer and the third one corresponds to the dense dip-coated LSCF layer. The adherence between layers is satisfactory, confirming macroscopic observations (Figure 3). The thickness of the CGO-Co interlayer is approximately 80 μm with randomly distributed porosity. However, it is not properly interconnected to provide enough gas diffusion routes. The outer LSCF dense layer presents a thickness of 30 μm and is well densified with virtually no defects, as shown in Figure 5d. The final grain size after sintering is around 8 μm .

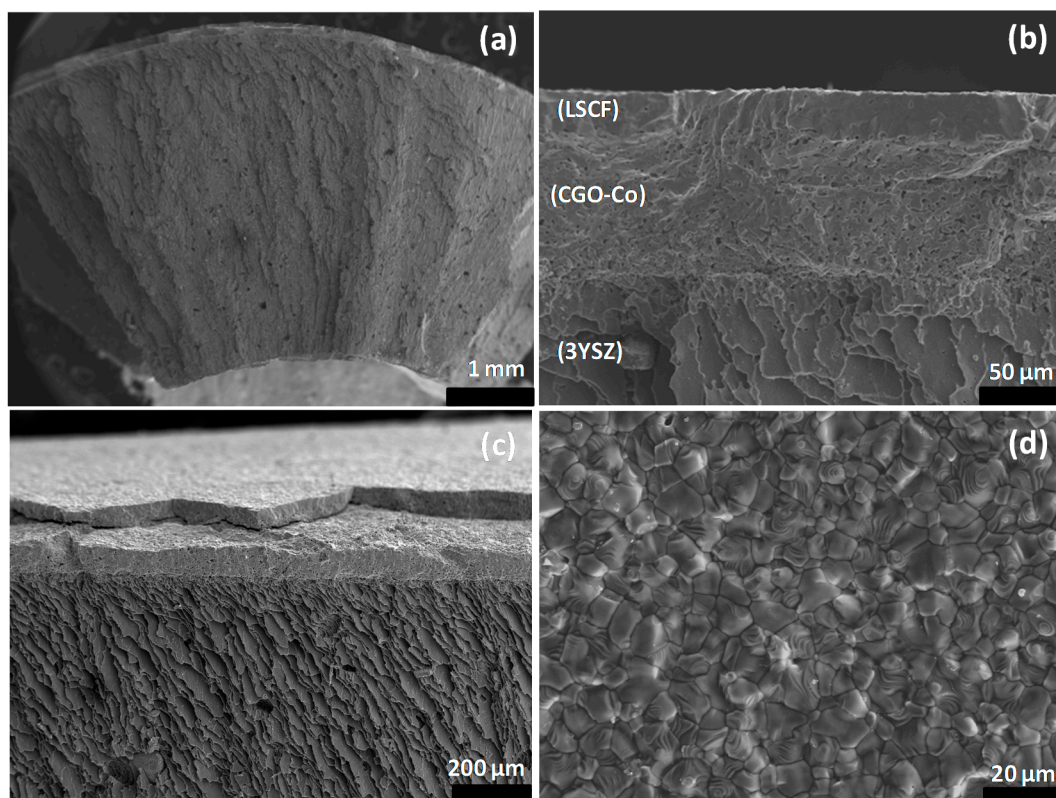


Figure 5. SEM micrographs of the radial surface of the tubular porous asymmetric membrane (a), cross section of the three distinct layers with the 3YSZ freeze-cast porous support, the CGO-Co porous interlayer and the LSCF dense top-layer (b,c) and surface of the LSCF dense top-layer (d).

In order to figure out if there is cation diffusion or unwanted reactions between phases in the membrane, EDX mapping was carried out in both layer boundaries. Figure 6 details the La, Fe, Ce elements distribution for the LSCF/CGO-Co interface (upper part) and the Ce, Zr and Y elements distribution for the CGO-Co/3YSZ interface (bottom part). Regarding the LSCF/CGO-Co interface, it is clearly noted that La and Fe present in the LSCF structure do not migrate to the CGO-Co layer in the same way that Ce cations are not transferred to the LSCF structure, despite the high sintering temperatures. This reactivity between phases had already been reported for both materials at 1200 °C/36 h and no interaction was registered [23]. It seems that both materials present an excellent chemical compatibility up to 1400 °C. The CGO-Co/3YSZ interface does not yield chemical reactivity between both materials. Indeed, Ce, Zr, and Y cations remain in the CGO-Co and 3YSZ layers, respectively. Even though no cation migration from one structure to the other was detected by EDX, there is not enough evidence to assure that there is no interaction, hence a thorough characterization is needed in order to assert complete stability between both phases. Nevertheless, the absence in reactivity detected is compelling.

Additional characterization by XRD analysis was performed at different stages of the elaboration process to verify the previous observations. As an intermediate characterization, an XRD analysis was realized over the dip-coated CGO-Co interlayer after a sintering treatment at 1150 °C/3 h over a freeze-cast 3YSZ tubular support. Figure 7 shows the patterns equivalent to the CGO-Co starting powder and the CGO-Co interlayer after 3 h at 1150 °C. The CGO-Co interlayer pattern after sintering is similar to the CGO-Co starting powder pattern. No additional phase is observable in the limit of the XRD detection. It is worthy to note that at this stage of the process, no cracks or delamination of the CGO-Co layer can be perceived.

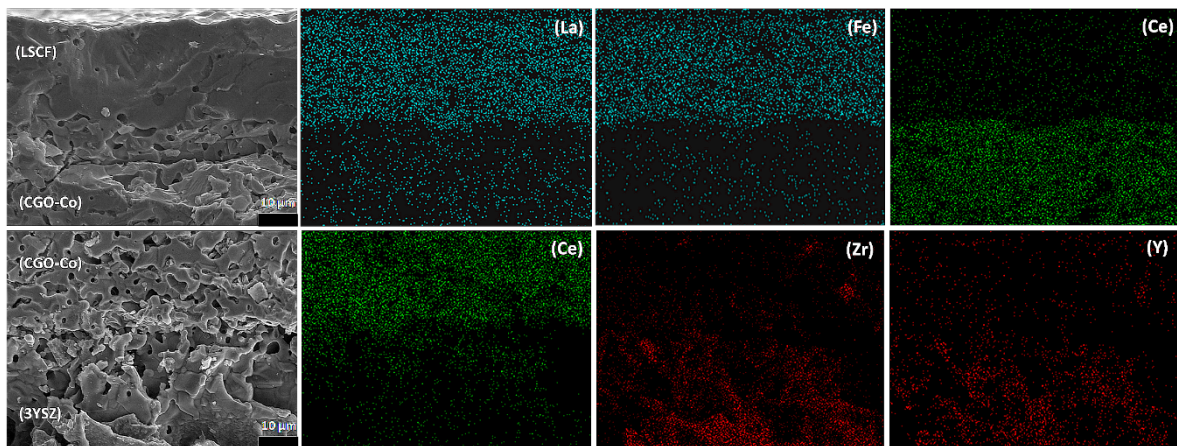


Figure 6. Elements distribution by EDX mapping for the CGO-Co/LSCF interface (upper part) and for the CGO-Co/3YSZ interface (bottom part).

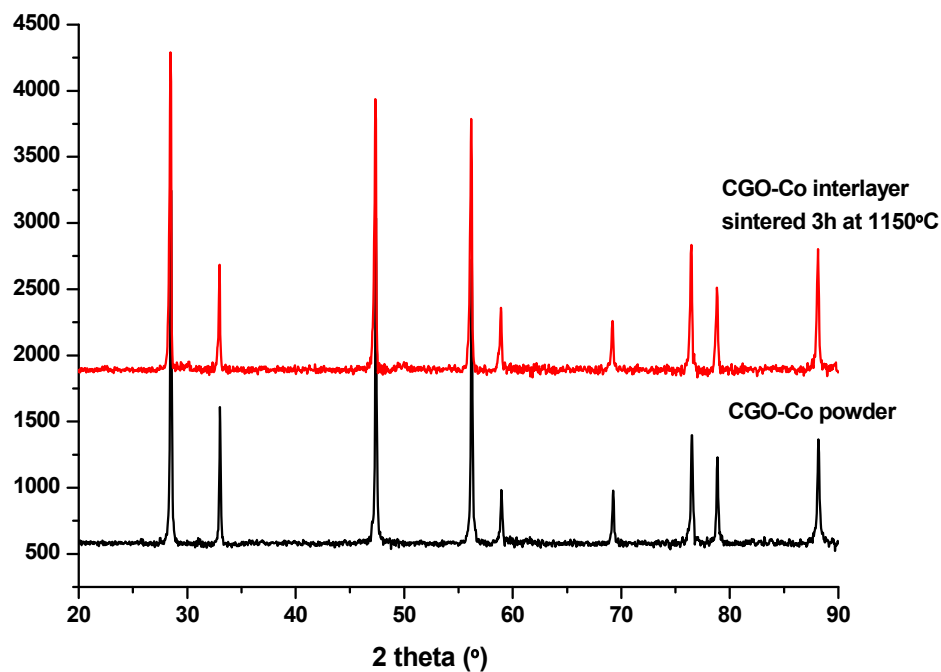


Figure 7. XRD patterns of the CGO-Co starting powder and the intermediate CGO-Co interlayer after sintering at 1150 °C/3 h.

After manufacturing a complete tubular asymmetric membrane, a final XRD analysis was performed on the outer surface of the sample (LSCF dense top-layer) to check the correspondence with its perovskite phase pattern and the absence of undesired phases. As shown in Figure 8, the outer LSCF layer presents only the LSCF phase with no secondary phases or anomalous peaks.

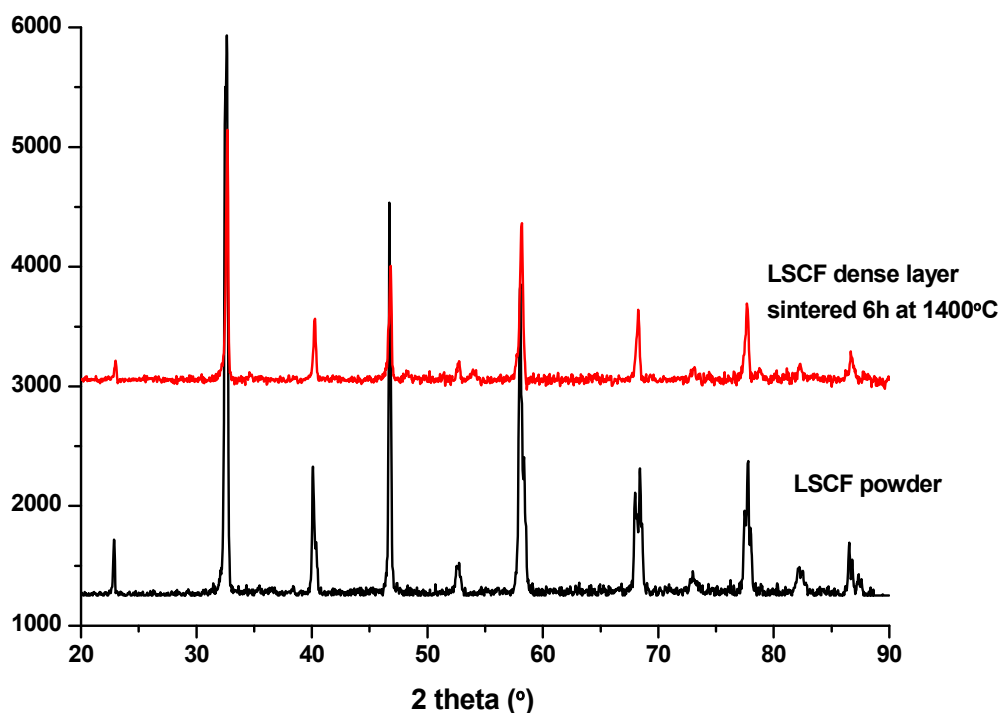


Figure 8. XRD patterns of the LSCF starting powder and of the LSCF dense top-layer after sintering 6 h at 1400 °C.

5. Oxygen Permeation Evaluation

The final asymmetric tubular freeze-cast membrane was assessed for the first time for oxygen permeation. Figure 9a represents the evolution of the oxygen permeation as a function of temperature between 850 °C and 1000 °C when air and argon are supplied as feed and sweep gases respectively (flow rate: 300 mL·min⁻¹). It can be seen that oxygen permeation increases with temperature and reaches 0.31 mL·min⁻¹·cm⁻² at 1000 °C while it is of 0.08 mL·min⁻¹·cm⁻² at 850 °C. The obtained results are far from the expected performance as previously reported in planar all-LSCF membranes deposited on freeze-cast [6,31] and tape-cast [5] porous supports, where oxygen fluxes of 6.8 and 4.3 mL·min⁻¹·cm⁻² were obtained for 30 μm-thick membranes. Instead, the tested tubular membrane presents a similar performance to the data observed in a 40 μm-thick asymmetric CGO-Co membrane [32], as can be seen in Figure 9a. This can be ascribed to a low porosity of the 80 μm-thick CGO-Co layer (Figure 5), which impedes feed gas diffusion to the LSCF layer, becoming a hindrance for oxygen permeation. The obtained results fit to an Arrhenius law where the apparent activation energy (E_a) gives 113.5 ± 5 kJ·mol⁻¹, being almost coincident to the E_a calculated for the CGO-Co membrane (123.9 ± 1.3 kJ·mol⁻¹) and much higher than that expected for a LSCF membrane material in this temperature range [6,8], fluctuating around 70 kJ·mol⁻¹. The latter supports the fact that oxygen permeation is limited by the bulk diffusion through the CGO-Co layer in the studied tubular membrane, thus reducing significantly the potential oxygen production capability. Another important aspect in oxygen production is the use of higher pressures in the air feed to increase the oxygen production. This is based on the fact that oxygen permeation is governed by Wagner's equation ($J_{O_2} = \frac{RT}{16F^2L} \int_{p''_{O_2}}^{p'_{O_2}} \sigma_{amb}(p_{O_2}) d \ln p_{O_2}$, where J_{O_2} is the oxygen permeation flux in mol·m⁻²·s⁻¹, R is the gas constant, F is the Faraday constant, L is the membrane thickness, σ_{amb} is the ambipolar conductivity, and p'_{O_2} and p''_{O_2} are the oxygen partial pressures at the high pressure side and low pressure side, respectively.) and surface exchange [33] at these temperatures. For the first, it is established a J_{O_2} direct dependence on p_{O_2} gradient between feed and permeate sides, in the way that increasing Δp_{O_2} by using pressurized feeds will result in an increase in oxygen permeation. Due to the experimental set limitations and the impossibility to use pressurized streams, this was simulated by increasing

pO_2 in the feed stream, as shown in Figure 9b. Specifically, Figure 9b presents the variation in J_{O_2} as a function of pO_2 at 1000 °C. At this temperature, J_{O_2} increases linearly with pO_2 and reaches a value of $1.07 \text{ mL}\cdot\text{min}^{-1}\cdot\text{cm}^{-2}$ under pure oxygen, which would correspond to a 5 bar air feeding. Again, these values are close to the obtained for the asymmetric CGO-Co membrane [32], and much lower than the $17.5 \text{ mL}\cdot\text{min}^{-1}\cdot\text{cm}^{-2}$ obtained with a planar LSCF freeze-cast membrane under similar conditions [6]. Figure 9c depicts the evolution of O_2 permeation flux as a function of the feed (air) flow rate at 1000 °C. For this scenario, the oxygen permeation increases linearly with the increase of the inlet flow for values lower than $150 \text{ mL}\cdot\text{min}^{-1}$ where it is of $0.22 \text{ mL}\cdot\text{min}^{-1}\cdot\text{cm}^{-2}$. For higher inlet flow, the oxygen permeation follows a parabolic trend and reaches $0.26 \text{ mL}\cdot\text{min}^{-1}\cdot\text{cm}^{-2}$ for an inlet flow of $300 \text{ mL}\cdot\text{min}^{-1}$. This trend can be explained by the increase in polarization resistance at high inlet flux caused by the random porosity of the CGO-Co interlayer, thus affecting the driving force. In comparison with permeation results in asymmetric LSCF membranes produced by freeze-casting and tape-casting, values of this tubular membrane remain low [5,6,8,31]. This gap can be explained by (i) the presence of the CGO-Co interlayer which presents a non-optimized porosity. Indeed, as it can be seen Figure 5b, the layer is porous, but its random organization does not facilitate gas transport to the LSCF dense top-layer; (ii) the thickness of the 3YSZ support: Despite a hierarchical porous organization, the porous support remains quite thick (Figure 5a), inducing gas transport limitations.

Even though the tubular membrane displays a low oxygen permeation, there are different, straightforward ways to improve its performance. To begin, an increase in the porosity of the CGO-Co interlayer would increase the amount of air that reaches the MIEC separation layer, enhancing the overall yield of the membrane. This can be achieved by introducing a certain amount of an organic pore former to the CGO-Co slurry that will decompose during the thermal treatment [34]. Secondly, a reduction in the thickness of the interlayer (CGO-Co) or the MIEC layer (LSCF-CGO) would also increase the oxygen permeation flux, as it is described by Wagner's equation, where J_{O_2} is inversely proportional to the thickness of the layer. Thirdly, adjusting the composition of the support slurry would allow an increase in the porosity and a consequent increase in the air flux reaching the MIEC separation layer. Fourthly, the addition of an external porous catalytic layer composed by LSCF would increase the surface area for the O_2 gas exchange, maximizing the membrane permeation [5,35]. Fifthly, a reduction of the support thickness would offer less resistance to air flow, while diminishing the membrane mechanical strength. For this, an acceptable trade-off between both properties must be attained.

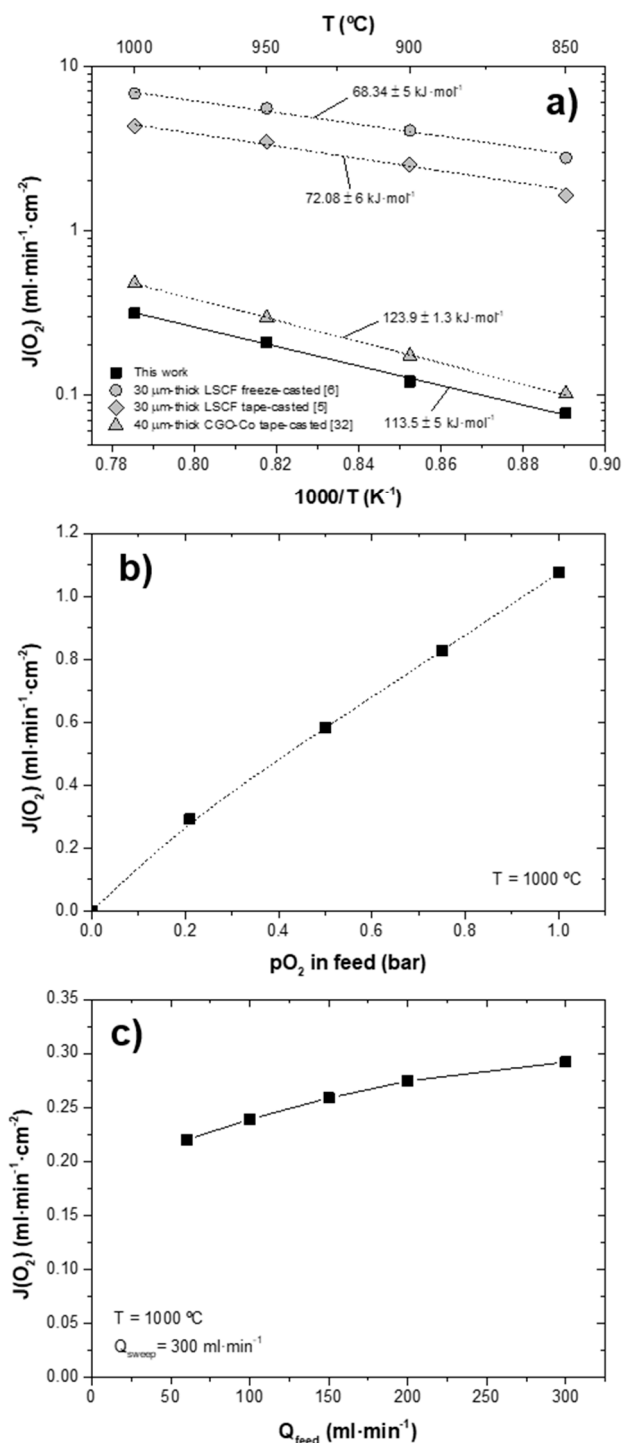


Figure 9. Oxygen permeation flux through the tubular freeze-cast asymmetric membrane (a) as a function of temperature (added permeation results of asymmetric LSCF and CGO-Co membranes for comparison), (b) as a function of $p\text{O}_2$ in the feed flow at $1000 \text{ }^\circ\text{C}$. Sweep gas: $300 \text{ mL}\cdot\text{min}^{-1}$ argon and (c) as a function of the feed inlet flux at $1000 \text{ }^\circ\text{C}$. Sweep gas: $300 \text{ mL}\cdot\text{min}^{-1}$ argon.

6. Conclusions

The innovative ice-templating or freeze-casting process has been implemented for the elaboration of a 3YSZ porous tubular support that exhibits hierarchical and radial-oriented porosity with fully densified walls approximately $2 \mu\text{m}$ thick, spaced by void regions around $15 \mu\text{m}$ wide. Such support was successively dip-coated with a CGO-Co-based slurry followed by a LSCF-based slurry. The $80 \mu\text{m}$

thick CGO-Co interlayer was effectively applied to avoid reported chemical interaction between the 3YSZ support and the LSCF outer dense layer. This external LSCF layer presents a thickness of 30 μm and is fully densified by a final sintering treatment at 1400 °C. A full microscopic study coupled with XRD analysis at different stages of the manufacturing process have discarded the chemical incompatibility between the three layers of the membrane and confirmed its compatibility for pure oxygen production. Finally, such a membrane has been evaluated for oxygen permeation and is reported for the first time, despite low values in comparison with previous freeze-cast membranes, ascribed to the non-optimal porosity degree of the CGO-Co layer. Regarding an upscaling of the production process, the diameter of the tube and the thickness of its walls are critical parameters during ice growth in the 3YSZ support. Therefore, both parameters should be preserved during industrial upscaling and commercialization. However, the length of the tubes does not become a constraint throughout the industrial manufacturing process, allowing the production of longer tubes in pursuance of an increase in oxygen permeation fluxes and a more compact design of the setup. Doing so, there are fewer parameters that will set back an upscaling of the process. Nevertheless, results appear to be promising since it was the first freeze-cast asymmetric membrane manufactured in a tubular configuration to be tested. Improvements regarding material selection and microstructure of slip-cast ion-conducting layers can be achieved, leading to higher oxygen permeation fluxes.

Author Contributions: Investigation, C.G., J.G.-F., J.P. and J.M.S.; methodology, J.M.S.; supervision, J.M.S.; writing—original draft, C.G., J.G.-F. and J.P.; writing—review and editing, J.M.S.

Funding: This research was funded by the Spanish Government, grant number ENE2014-57651 and SEV-2016-0683.

Acknowledgments: Funding from the Spanish Government (ENE2014-57651 and SEV-2016-0683 grants) is kindly acknowledged.

Conflicts of Interest: The authors declare no conflict of interest.

References

1. Hashim, S.S.; Mohamed, A.R.; Bhatia, S. Oxygen separation from air using ceramic-based membrane technology for sustainable fuel production and power generation. *Renew. Sustain. Energy Rev.* **2011**, *15*, 1284–1293. [[CrossRef](#)]
2. Bredesen, R.; Sogge, A. A technical and economic assessment of membrane reactors for hydrogen and syngas production. In Proceedings of the Seminar on the Ecological Applications of Innovative Membrane Technology in the Chemical Industry, Cetraro, Italy, 1 May 1996 .
3. Den Exter, M.; Haije, W.; Vente, J. Viability of ITM Technology for Oxygen Production and Oxidation Processes: Material, System, and Process Aspects. In *Inorganic Membranes for Energy and Environmental Applications*; Bose, A., Ed.; Springer: New York, NY, USA, 2009; pp. 27–51.
4. Rajesh, S.; Pereira, J.R.S.; Figueiredo, F.M.L.; Marques, F.M.B. Performance of Carbonate—LaCoO₃ and La_{0.8}Sr_{0.2}Co_{0.2}Fe_{0.8}O_{3- δ} Composite Cathodes under Carbon Dioxide. *Electrochim. Acta* **2014**, *125*, 435–442. [[CrossRef](#)]
5. Serra, J.M.; Garcia-Fayos, J.; Baumann, S.; Schulze-Küppers, F.; Meulenberg, W.A. Oxygen permeation through tape-cast asymmetric all-La_{0.6}Sr_{0.4}Co_{0.2}Fe_{0.8}O_{3- δ} membranes. *J. Membr. Sci.* **2013**, *447*, 297–305. [[CrossRef](#)]
6. Gaudillere, C.; Garcia-Fayos, J.; Serra, J. Enhancing oxygen permeation through hierarchically-structured perovskite membranes elaborated by freeze-casting. *J. Mater. Chem. A* **2013**. [[CrossRef](#)]
7. Deville, S. Freeze-casting of porous ceramics: A review of current achievements and issues. *Adv. Eng. Mater.* **2008**, *10*, 155–169. [[CrossRef](#)]
8. Gaudillere, C.; Garcia-Fayos, J.; Balaguer, M.; Serra, J.M. Enhanced Oxygen Separation through Robust Freeze-Cast Bilayered Dual-Phase Membranes. *ChemSusChem* **2014**, *7*, 2554–2561. [[CrossRef](#)] [[PubMed](#)]
9. Hong, L.; Chua, W. Fabrication of a dense La_{0.2}Sr_{0.8}CoO_{3- δ} /CoO composite membrane by utilizing the electroless cobalt plating technique. *J. Membr. Sci.* **2002**, *198*, 95–108. [[CrossRef](#)]

10. Middleton, H.; Diethelm, S.; Ihringer, R.; Larrain, D.; Sfeir, J.; Van Herle, J. Co-casting and co-sintering of porous MgO support plates with thin dense perovskite layers of LaSrFeCoO₃. *J. Eur. Ceram. Soc.* **2004**, *24*, 1083–1086. [[CrossRef](#)]
11. Lee, T.H.; Yang, Y.L.; Jacobson, A.J.; Abeles, B.; Zhou, M. Oxygen permeation in dense SrCo_{0.8}Fe_{0.2}O₃— δ membranes: Surface exchange kinetics versus bulk diffusion. *Solid State Ionics* **1997**, *100*, 77–85. [[CrossRef](#)]
12. Balachandran, U.; Dusek, J.T.; Maiya, P.S.; Ma, B.; Mieville, R.L.; Kleefisch, M.S.; Udovich, C.A. Ceramic membrane reactor for converting methane to syngas. *Catal. Today* **1997**, *36*, 265–272. [[CrossRef](#)]
13. Balachandran, U.; Dusek, J.T.; Mieville, R.L.; Poeppel, R.B.; Kleefisch, M.S.; Pei, S.; Kobylinski, T.P.; Udovich, C.A.; Bose, A.C. Dense ceramic membranes for partial oxidation of methane to syngas. *Appl. Catal. A Gener.* **1995**, *133*, 19–29. [[CrossRef](#)]
14. Li, S.; Jin, W.; Huang, P.; Xu, N.; Shi, J.; Lin, Y.S. Tubular lanthanum cobaltite perovskite type membrane for oxygen permeation. *J. Membr. Sci.* **2000**, *166*, 51–61. [[CrossRef](#)]
15. Liu, Z.; Zhang, G.; Dong, X.; Jiang, W.; Jin, W.; Xu, N. Fabrication of asymmetric tubular mixed-conducting dense membranes by a combined spin-spraying and co-sintering process. *J. Membr. Sci.* **2012**, *415–416*, 313–319. [[CrossRef](#)]
16. Ito, W.; Nagai, T.; Sakon, T. Oxygen separation from compressed air using a mixed conducting perovskite-type oxide membrane. *Solid State Ionics* **2007**, *178*, 809–816. [[CrossRef](#)]
17. Zhu, X.; Sun, S.; Cong, Y.; Yang, W. Operation of perovskite membrane under vacuum and elevated pressures for high-purity oxygen production. *J. Membr. Sci.* **2009**, *345*, 47–52. [[CrossRef](#)]
18. Moon, J.W.; Hwang, H.J.; Awano, M.; Maeda, K. Preparation of NiO-YSZ tubular support with radially aligned pore channels. *Mater. Lett.* **2003**, *57*, 1428–1434. [[CrossRef](#)]
19. Moon, Y.W.; Shin, K.H.; Koh, Y.H.; Yook, S.W.; Han, C.M.; Kim, H.E. Novel ceramic/camphene-based co-extrusion for highly aligned porous alumina ceramic tubes. *J. Am. Ceram. Soc.* **2012**, *95*, 1803–1806. [[CrossRef](#)]
20. Liu, R.; Yuan, J.; Wang, C.A. A novel way to fabricate tubular porous mullite membrane supports by TBA-based freezing casting method. *J. Eur. Ceram. Soc.* **2013**, *33*, 3249–3256. [[CrossRef](#)]
21. Seub, J.; Leloup, J.; Richaud, S.; Deville, S.; Guizard, C.; Stevenson, A.J. Fabrication of ice-templated tubes by rotational freezing: Microstructure, strength, and permeability. *J. Eur. Ceram. Soc.* **2017**, *37*, 2423–2429. [[CrossRef](#)]
22. Knibbe, R.; Hjelm, J.; Menon, M.; Pryds, N.; Søgaard, M.; Wang, H.J.; Neufeld, K. Cathode–Electrolyte Interfaces with CGO Barrier Layers in SOFC. *J. Am. Ceram. Soc.* **2010**, *93*, 2877–2883. [[CrossRef](#)]
23. Qiu, L.; Ichikawa, T.; Hirano, A.; Imanishi, N.; Takeda, Y. Ln_{1-x}Sr_xCo_{1-y}FeyO_{3- δ} (Ln = Pr, Nd, Gd; x = 0.2, 0.3) for the electrodes of solid oxide fuel cells. *Solid State Ionics* **2003**, *158*, 55–65. [[CrossRef](#)]
24. Zhou, X.D.; Scarfino, B.; Anderson, H.U. Electrical conductivity and stability of Gd-doped ceria/Y-doped zirconia ceramics and thin films. *Solid State Ionics* **2004**, *175*, 19–22. [[CrossRef](#)]
25. Mori, M.; Hiei, Y.; Itoh, H.; Tompsett, G.A.; Sammes, N.M. Evaluation of Ni and Ti-doped Y₂O₃ stabilized ZrO₂ cermet as an anode in high-temperature solid oxide fuel cells. *Solid State Ionics* **2003**, *160*, 1–14. [[CrossRef](#)]
26. Antunes, B.C. Production of Volumetric Ceramic Porous Burners by Direct Foaming Process. Ph.D. Thesis, University of Bremen, Advanced Ceramics Institute, Bremen, Germany, 2010.
27. Schulze-Küppers, F.; Baumann, S.; Tietz, F.; Bouwmeester, H.J.M.; Meulenber, W.A. Towards the fabrication of La_{0.98-x}Sr_xCo_{0.2}Fe_{0.8}O_{3- δ} perovskite-type oxygen transport membranes. *J. Eur. Ceram. Soc.* **2014**, *34*, 3741–3748. [[CrossRef](#)]
28. Pérez-Coll, D.; Núñez, P.; Abrantes, J.C.C.; Fagg, D.P.; Kharton, V.V.; Frade, J.R. Effects of firing conditions and addition of Co on bulk and grain boundary properties of CGO. *Solid State Ionics* **2005**, *176*, 2799–2805. [[CrossRef](#)]
29. Baque, L.; Padmasree, K.P.; Reyes, M.A.C.; Troiani, H.; Arce, M.D.; Serquis, A.; Soldati, A. Effect of Cobalt-Doped Electrolyte on the Electrochemical Performance of LSCFO/CGO Interfaces. *ECS Trans.* **2016**, *72*, 117–121. [[CrossRef](#)]
30. Balaguer, M.; Solis, C.; Roitsch, S.; Serra, J.M. Engineering microstructure and redox properties in the mixed conductor Ce_{0.9}Pr_{0.1}O_{2- δ} + Co 2 mol%. *Dalton Trans.* **2014**, *43*, 4305–4312. [[CrossRef](#)]

31. Gaudillere, C.; Garcia-Fayos, J.; Serra, J.M. Oxygen Permeation Improvement under CO₂-Rich Environments through Catalytic Activation of Hierarchically Structured Perovskite Membranes. *ChemPlusChem* **2014**, *79*, 1720–1725. [[CrossRef](#)]
32. Garcia-Fayos, J.; Søggaard, M.; Kaiser, A.; Serra, J.M. Oxygen permeation studies in surface Pd-activated asymmetric Ce_{0.9}Gd_{0.1}O_{1.95} membranes for application in CO₂ and CH₄ environments. *Sep. Purif. Technol.* **2019**, *216*, 58–64. [[CrossRef](#)]
33. Bouwmeester, H.; Burggraaf, A. Dense Ceramic Membranes for Oxygen Separation. In *Handbook of Solid State Electrochemistry*; CRC Press: Boca Raton, FL, USA, 1997. [[CrossRef](#)]
34. Escribano, J.A.; García-Fayos, J.; Serra, J.M. Shaping of 3YSZ porous substrates for oxygen separation membranes. *J. Eur. Ceram. Soc.* **2017**, *37*, 5223–5231. [[CrossRef](#)]
35. Lobera, M.P.; Balaguer, M.; García-Fayos, J.; Serra, J.M. Catalytic Oxide-Ion Conducting Materials for Surface Activation of Ba_{0.5}Sr_{0.5}Co_{0.8}Fe_{0.2}O_{3-δ} Membranes. *ChemistrySelect* **2017**, *2*, 2949–2955. [[CrossRef](#)]



© 2019 by the authors. Licensee MDPI, Basel, Switzerland. This article is an open access article distributed under the terms and conditions of the Creative Commons Attribution (CC BY) license (<http://creativecommons.org/licenses/by/4.0/>).